



Structural, Optical, Mechanical and Antibacterial Properties of MgO/Poly(Vinyl Acetate)/Poly(Vinyl Chloride) Nanocomposites

Adel M. El Sayed¹  · A. M. Abdelghany² · A. Abou Elfadl¹ 

Received: 18 April 2022 / Accepted: 15 June 2022
© The Author(s) 2022

Abstract

Polymeric blends and nanocomposites with improved functional properties have attracted attention worldwide for industrial applications. For food packaging applications and carrying purposes, the materials to be used should have UV blocking ability, antibacterial activity, and good mechanical properties. In this study, polyvinyl acetate (PVAc)/polyvinyl chloride (PVC) blends with optimized properties and MgO/PVAc/PVC polymer nanocomposites (PNCs) were prepared by solution casting and evaporation. Fourier transform infrared (FTIR) spectroscopy confirmed the complexation and miscibility between PVAc and PVC and their interaction with MgO nanoparticles (NP). X-ray diffraction and HR-TEM analyses showed the phase purity of MgO NP with a crystallite size of ~ 18.8 nm and their dispersion in the amorphous regions of the blend without affecting the structure of each other. UV–vis-NIR spectroscopy revealed that the band gap of the blend can be tuned by changing the added ratio of each polymer, and loading MgO NP increased the semiconducting behavior of the blend. Various optical constants such as the refractive index, absorption index, and optical dispersion parameters have been evaluated. The blend composition and effects of MgO content on the stress–strain behavior were studied. The addition of MgO to the blend enhanced the tensile modulus and strength. However, there was a corresponding decline in toughness and elongation at break. These results reflect the reinforcing effect of MgO NP, which reduces the flexibility of the polymer chains. The antibacterial activities of MgO/PVAc/PVC PNCs against *Staphylococcus aureus*, *Escherichia coli*, and *Candida albicans* fungi are studied. The improvements in optical, mechanical, and antimicrobial properties make these nanocomposites suitable for some optical devices and in food packaging applications.

Keywords PVAc/PVC blend · MgO · Optical constants · Stress–strain behavior · UV/Vis · Antibacterial activity

1 Introduction

Recent approaches have been developed to produce polymeric materials for advanced scientific and industrial purposes. The physical blending of two or more polymers is a simple and effective method to obtain components with improved physicochemical properties compared with the copolymerization and chemical routes [1]. On the other hand, the incorporation of a nano-sized material at specific

doping ratios can yield nanocomposites of tailored properties [2]. The reinforcement of the nano-fillers depends on their concentration in the matrix. The nano-sized fillers inside the polymer provide a high surface interaction between the filler and the chains of the polymer. This enhances the stress transfer from the chains to the nano-fillers, which results in an improvement in mechanical properties. However, due to the high surface energy of the nano-sized material, when its content exceeds a certain limit, its particles tend to agglomerate. This decreases the effective content of these fillers inside the matrix, where the agglomerated particles act as defects in the polymer network. This limits our expectation for more improvements in the properties of the resulting composites [3].

Poly(vinyl acetate), PVAc, is one of the amorphous biodegradable and transparent polymers that has a glass transition temperature of 30 °C, a melting point in the range of 70–210 °C, and can be used as a binder, paper finishing

✉ Adel M. El Sayed
ams06@fayoum.edu.eg

✉ A. Abou Elfadl
azzaaboelfadl@yahoo.com

¹ Physics Department, Faculty of Science, Fayoum University, El-Fayoum 63514, Egypt

² Spectroscopy Department, Physics Research Institute, National Research Centre, Giza 12311, Dokki, Egypt

agent, adhesive, and in different industrial branches, such as in microelectronic applications and antibacterial activity against *Staphylococcus aureus* (*S. aureus*). Moreover, its utilization can be broadened by blending with other polymers and/or by doping with nano-sized materials [1, 4–8]. Hammami et al. [5] reported that introducing cellulose nanocrystals (CNC) into PVAc hindered the PVAc chain's mobility and decreased its activation energy from 2.09 to 0.85 eV at 10 wt% CNC content, indicating the formation of a conductive network for charge carrier transportation. Khan et al. [7] fabricated Ag/GO/PVAc nanocomposites with improved conductivity for humidity sensing applications.

On the other hand, poly(vinyl chloride), PVC, is the third most widely produced polymeric material. It is characterized by various physical and chemical properties, including thermal stability, elasticity, high mechanical strength, transparency, and good insulation [4], making it safe for use in medical instruments, blood bags, and surgical dressings. The structure, optical bandgap tuning, and biological properties of PVAc/PVC blends of different compositions, as well as the influence of polyfuran and Fe₃O₄ NP on the conductivity, thermal, and magnetic properties of this blend, have been reported [4, 9].

Magnesium oxide (MgO) is an interesting nano-filler that can be used to induce nanocomposites with improved optical, mechanical, and biological properties. Besides the low cost, high-temperature stability, electrical insulation, UV blocking ability, and the high surface area of the nano-sized MgO, the oxygen vacancies make it capable of converting the dissolved oxygen in the water to O₂ anion free radical able to destroy bacteria cells and protein-peptide, i.e., MgO has a strong antimicrobial activity [10]. Moreover, MgO NP are non-toxic biomaterials because they can be degraded in the body. 2.0 wt% MgO-doped polylactic acid achieved progressive damage and death of ~46% of *Escherichia coli* (*E-Coli*) bacterial culture after 12 h treatment [3]. The released products (Mg²⁺ & OH⁻) of the degraded MgO can be easily eliminated from the body provided that the renal function is normal [11]. Doping MgO into the starch/albumin films induced halos of 4–6 mm in diameter against *E. coli* and *S. aureus* bacteria, demonstrating its antimicrobial properties [12].

Based on the above-mentioned survey, the physical properties of PVAc/PVC blends and the influence of MgO NP on the optical constants, mechanical and antimicrobial properties of this blend have not been reported. This work focuses on searching for an optimized composition of the PVAc/PVC blend (i.e., PVAc/PVC ratio) to be used as a host for different MgO NP doping ratios. Various physical properties of the samples were studied. Besides, the optical, mechanical, and antibacterial properties of MgO/PVAc/PVC were evaluated in the scope of their usage in practical applications such as carrying purposes and food packaging applications. MgO

NP was prepared by a sol–gel process and incorporated into the PVAc/PVC blend using the solution casting and evaporation technique. These synthetic methods are facile, cost-effective, and not time-consuming.

2 Experimental Section

2.1 Materials and Preparation

Poly(vinyl acetate) PVAc from Alpha Chemika, India, poly(vinyl chloride); PVC from Polymer Laboratories, Ltd. Essex, and tetrahydrofuran THF from Aldrich, Germany, were used for polymeric films preparation, where THF was used as a common solvent. On the other hand, a high purity magnesium acetate [Mg (CH₃COO)₂·4H₂O with molecular weight (M_w)=214.45 g/mol, from Nova Oleochem Limited, was used for preparing nano-sized MgO, where the oxalic acid (OA) [H₂C₂O₄·2H₂O, M_w=126.07 g/mol, from LOBA Chemie] was used as a chelating agent and the double-distilled water (DD) was used as a solvent.

Firstly, a 0.75-M solution was prepared by dissolving about 16.1 g of the acetate salt in 100 ml of DD. After ~10 min of the magnetic stirring process, 9.46 g of OA was added to this solution and the stirring continued for 1.0 h at 50 °C. The obtained sol was held in an air oven at 100 °C to evaporate the excess water and then aged for more than 18 h before the final annealing at 500 °C to obtain MgO. 2 g of PVC, PVAc, PVAc (30%)/PVC (70%), PVAc (50%)/PVC (50%), and PVAc (70%)/PVC (30%), each was dissolved in 75 ml THF under stirring at 60 °C for 30 min in tightly closed beakers and the stirring was continued for another 30 min at room temperature (RT). To prepare nanocomposite films, the PVAc (50%)/PVC (50%) solution was doped with $x=3.0, 5.0,$ and 10.0 wt% of the sol–gel prepared MgO. The required mass (w_f) of MgO fillers was determined using the following equation: $(xwt\%) = \frac{w_f}{w_f+2} \times 100$, where 2 in the denominator is the total mass of the blend. The w_f was dissolved in 10 ml THF using ultrasonication and then added to the blend solution during the stirring process. The PVAc, PVC, PVAc/PVC, and MgO/PVAc/PVC solutions were put in Petri dishes and left for a complete day (24 h) for the solvent to be completely evaporated.

2.2 Characterization of Studied Samples

FTIR (Fourier transform infrared) absorption spectra in the wavenumber range of 4000–400 cm⁻¹ were recorded for all samples by using a Bruker Vertex 70 Spectrophotometer coupled with a diamond attenuated total reflection unit. X-ray diffraction (XRD) patterns of MgO, PVAc (50%)/PVC (50%) blend, and MgO/blend nanocomposites were

recorded utilizing XRD, PANalytical X'PertPRO, with Cu K_{α} radiation of wavelength $\lambda = 0.1541$ nm, at RT and in the range of $2\theta = 4.0^{\circ} - 80.0^{\circ}$. A high-resolution (HR) transmission electron microscope (TEM; JEM 2100, Jeol), operated at 200 kV, was used to investigate the size and morphology of the prepared MgO powder. The surface morphology of MgO, PVAc/PVC, and 10 wt% MgO/ blend was investigated by the field emission scanning electron microscope (FE-SEM), (Carl ZEISS Sigma 500 VP, coupled with EDS). UV-vis spectra for all samples were recorded by using a UV-3600 UV-Vis-NIR Shimadzu Spectrophotometer in the wavelength (λ) range 200–1200 nm. The film thickness was determined by using a digital micrometer. The mechanical properties of the prepared samples were determined by applying a tensile test on a ZwickRoell mechanical testing instrument with a 1-kN load cell (model Z010 TN, Germany). Tests were performed at a speed of 50 mm/min at RT. For each sample, the average value of three measurements was considered. Antimicrobial activity measurements were elaborated via the disc minimum inhibition zone route, adopting two gram-negative and two gram-positive bacteria.

2.3 Antibacterial Studies

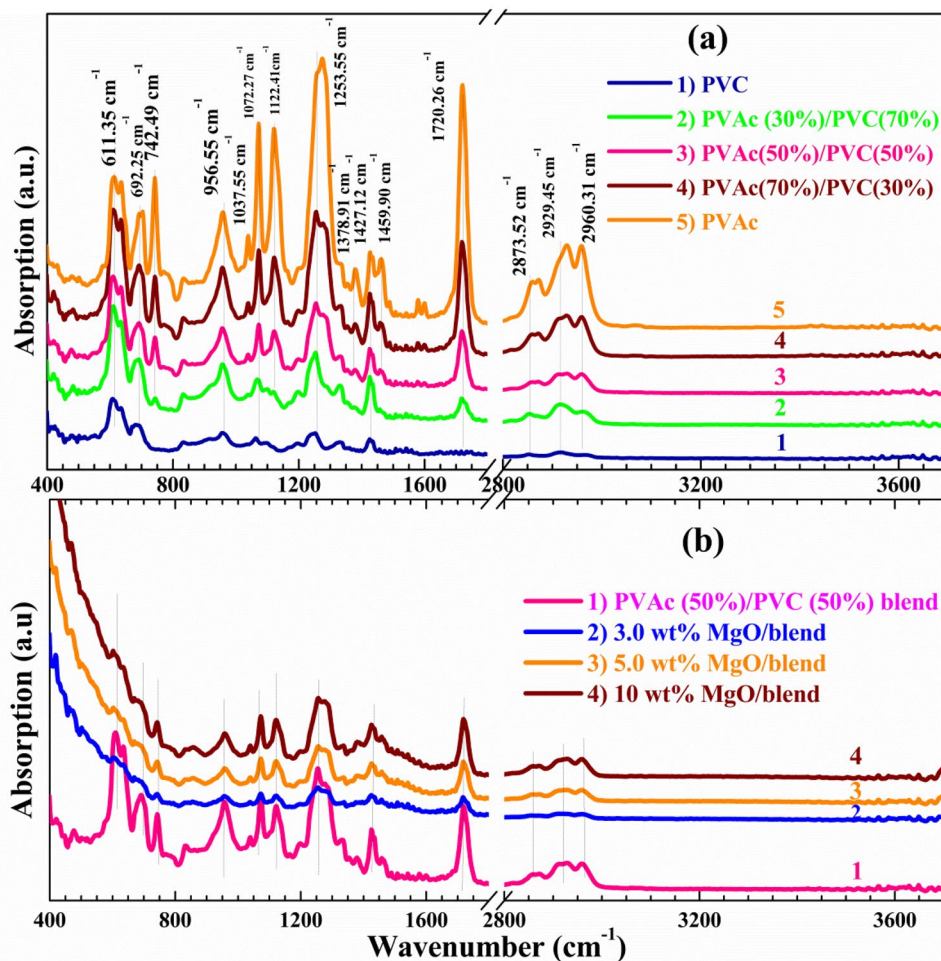
The antibacterial activity of the PVAc (50%)/PVC (50%) blend in combination with the blend containing variable content (3.0–10 wt%) of the synthesized MgO NP was inspected via an Agar diffusion test adopting *staphylococcus aureus* (*s. aureus*) gram-positive, *E-Coli* gram-negative, as well as (*Candida albicans*) fungi. The inhibition zone was retraced for three-replicated samples from each composition after 24 h and the standard error was calculated.

3 Results and Discussions

3.1 FTIR Spectroscopy, XRD Analysis, and Morphology

FTIR spectroscopy is an important method and a powerful characterization tool for the identification of the chemical functional groups of organic materials and their complexation via the induced excitation by IR radiation. Figure 1a shows the FTIR absorption spectra of PVC, PVAc, and

Fig. 1 FTIR absorption spectra of **a** PVC, PVAc, and their blends, **b** PVAc(50%)/PVC(50%) and their MgO nanocomposites



PVAc/PVC blends. The spectrum of PVC contains two small peaks at 2852 and 2960 cm^{-1} arising from the asymmetric and symmetric stretching of CH_2 , respectively [4], whereas the peak at 2916 cm^{-1} can be attributed to the stretching vibration of $\text{sp}^3\text{ C-H}$ bond [7]. The intensity of these peaks was enhanced with increasing PVAc content from 30 to 100%; moreover, the peaks were shifted to higher wavenumbers, as indicated in the figure. The acetate-ester absorbance band at 1720 cm^{-1} of the C=O (carbonyl group of PVAc) is strengthened with increasing PVAc content [8]. The band at 1427 cm^{-1} is the characteristic group of PVC, i.e., arising from the angular deformation of $\text{CH}_2\text{-Cl}$. The two peaks at 1460 and 1379 cm^{-1} refer to $\delta(\text{CH}_2)$ and $\delta(\text{CH}_3)$ of the PVAc, respectively [13]. These two peaks are not present in the spectrum of PVC and show continued growth with increasing the amount of PVAc in the blend.

Moreover, the peak at 1254 cm^{-1} became border and the most intense upon increasing the PVAc content, confirming the increase in the acetate structure of the blend [4]. The peak at 1122 cm^{-1} is owing to the vibration of the (C-C-C) and (C-C-O) bonds of PVAc. However, the bands at 1038 and 1072 cm^{-1} are owing to the C-C stretching vibration of PVAc and PVC, respectively, and their intensity increases with increasing PVAc content from 30 to 100%. The band at 957 cm^{-1} is due to C-H out-of-plane trans deformation [14]. In addition, the $\delta(\text{CH}_3\text{COO})$ vibration of PVAc appears at 742 cm^{-1} and continues to grow with PVAc addition. The C-Cl stretching vibration appears at 692 and 611 cm^{-1} [15]. These results confirm the presence of the functional groups of both PVC and PVAc with improving the frequency of PVC characteristic groups after blending with PVAc which is associated with the shifting of some peaks to higher wavenumbers.

Figure 1b shows the FTIR spectra of a PVAc (50%)/PVC (50%) blend loaded with different (3.0, 5.0, and 10 wt%) concentrations of MgO NP. The nanocomposites present similar peaks without any shifts but with reduced intensity, especially at 3.0 wt% MgO fillers content. Such a result indicates the complexation and interaction between MgO and the blend functional group. As seen, there is a reduction in the intensity of the peak at 742 cm^{-1} with MgO loading. The relative intensity I_r was estimated as the ratio of the area of a specific peak to the area of the whole spectrum in the wavenumber range of $500\text{--}3250\text{ cm}^{-1}$. The estimated I_r value of the peak at 742 cm^{-1} reduced from 2.71 for pure blend to 2.04, 2.21, and 2.23% with doping of 3.0, 5.0, and 10 wt% MgO, respectively, which confirms the formation of hydrogen bonding between the MgO and CH_3COO groups of the PVAc. In addition, the almost absence of the peaks at 692 and 611 cm^{-1} at 3 and 10 wt% MgO illustrates the dehydrochlorination effect and the ability of MgO to break the C-Cl bonds of PVC.

The XRD patterns for MgO powder, PVAc (50%)/PVC (50%) blend, and MgO/blend nanocomposites are shown in Fig. 2. XRD pattern of MgO contains five peaks at $2\theta = 36.86^\circ$, 42.78° , 62.25° , 74.45° , and 78.3° with corresponding Miller's indices (1 1 1), (2 0 0), (2 2 0), (3 1 1), and (2 2 2) planes, respectively. This result is consistent with the data of JCPDS Card No. 45-0946 for the cubic MgO (periclase phase). The average crystallite size D ($\sim 18.8\text{ nm}$) of MgO was calculated using the well-known Scherer's equation ($D = \frac{0.9\lambda}{\beta \cos\theta}$), where the wavelength $\lambda = 0.1541\text{ nm}$ ($\text{Cu K}\alpha$ radiation) and β is the full-width at half maximum intensity. The pure PVAc/PVC blend exhibits two halos; the first extends from 15° to 28° and the second peak is around 40° on the 2θ scale. These results reflect the amorphous nature of the two polymers and their blend. Abdelghany et al. [4] found three halos in the spectrum of PVC film at 17.7° , 24.7° , and 40.6° and two halos for PVAc film at 15.07° and 22.71° . The XRD pattern of PVAc was found to consist of two adjacent peaks around 13° and 22° forming a wide halo, and another less intense but broad peak at $\sim 45^\circ$ [5]. Similarly, two broad peaks in the region of $2\theta = 10\text{--}30^\circ$ were assigned to the PVAc [6]. Moreover, the XRD patterns of MgO/PVAc/PVC are similar to those of the pure blend but the peaks appear with enhanced intensity. In addition, the MgO peaks at 42.78° and 62° corresponding to (2 0 0) and (2 2 0) planes, appear superimposed on the blend spectrum. These results indicate that PVAc and PVC are well-miscible with each other and MgO is well distributed in the blend matrix [16] without affecting the structure of each other.

To check and investigate the sol-gel prepared MgO, apart from the 10.0 wt%/blend, the sample was dissolved in THF and a suspension solution was formed. HR-TEM image was

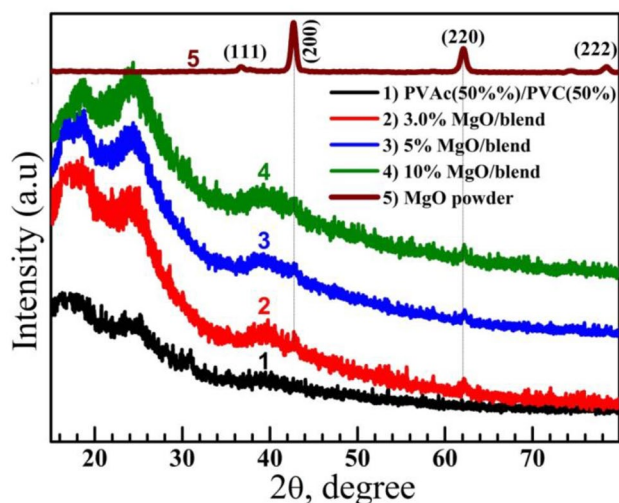


Fig. 2 XRD patterns of PVAc/PVC blend, the blend loaded with (3.0–10 wt% MgO), and the sol-gel prepared MgO powder

taken and shown in Fig. 3a. MgO appears as nearly spherical NP of various sizes, all less than 70 nm. The big particles seen in this image may result from the agglomeration of small particles inside the blend matrix. Finally, before proceeding with studying other physical properties of the materials, SEM images were taken and shown in Fig. 3. It seems that the blend displays a smooth and nonporous surface that is crack-free (Fig. 3b). The 10.0 wt% MgO-doped blend exhibits a similar surface but with some MgO agglomerations, see Fig. 3c, due to the high surface energy of the nano-sized fillers. For more details about the surface morphology and MgO NP distribution and agglomeration, other SEM images for the blend and 10 wt% MgO/blend were taken at higher magnification as shown in Fig. S1.

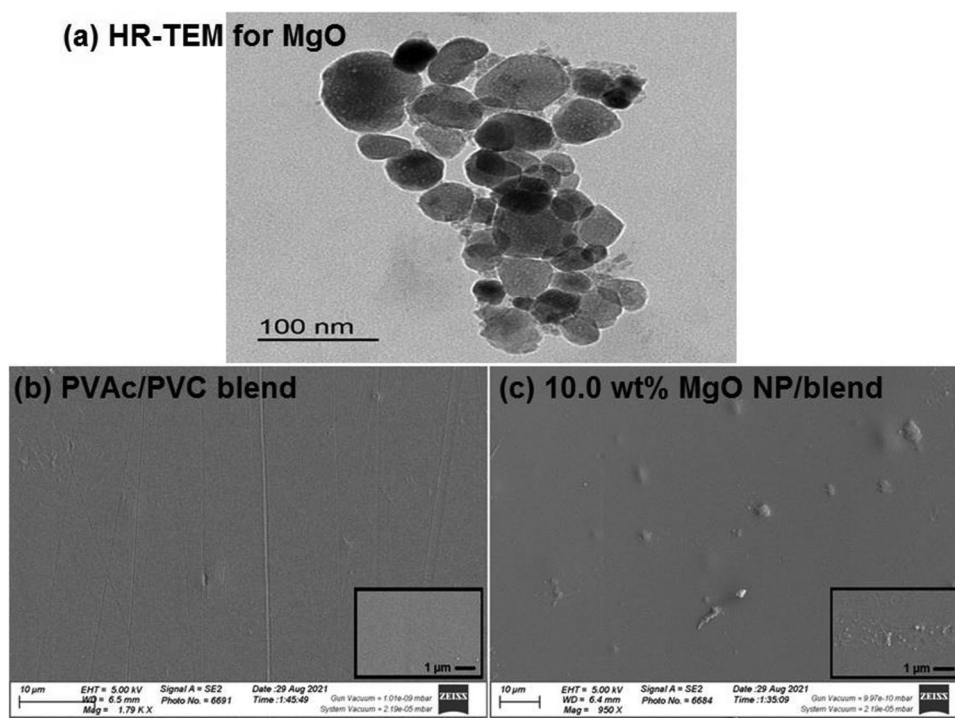
3.2 Optical Properties

The UV–vis–NIR, also known as electronic absorption spectroscopy, is a widely used technique to study the band structure of the material and electronic transitions between the ground state and the excited states upon absorption of wavelengths in the ultraviolet, visible, and infrared regions. Figure 4a displays the transmittance ($T\%$) spectra of PVC, PVAc, and the PVAc/PVC blends composed of different ratios; 30%/70%, 50%/50%, and 70%/30%. All films exhibit zero $T\%$ before $\lambda = 280$ nm, except the PVC film, which has an absorption band around $\lambda = 278$ nm. This band is appointed to $\pi \rightarrow \pi^*$ electronic transition. In addition, the increased absorbance at λ less than 256 nm is related to the

C–Cl bond [17]. In the visible and IR regions, PVC exhibits $T\%$ in the range of 80–85%. Similar values (82% in the region of 690–800 nm) were reported for PVC by ElSad et al. [18]. The value of $T\%$ at a 650 nm wavelength is listed in Table 1. As clearly seen, the blend of composition PVAc (50%)/PVC (50%) exhibits the highest $T\%$ value in the range of 83–90%. In addition, increasing PVAc content in the blend to 30, 70, and 100% shifts the absorption edge to a relatively longer wavelength.

The lost portion of the incident electromagnetic (photon) energy when passing through the PVAc, PVAc, the PVAc/PVC blends, and MgO/blend due to absorption and/or scattering effect is represented as the absorption index k ; $k = \frac{\alpha \lambda}{4\pi}$, where α (the absorption coefficient) = $\frac{2.303A}{t}$, A is the absorption and t is the film thickness. The k spectra of the polymeric samples are shown in Fig. 4b. The $\pi \rightarrow \pi^*$ transition in PVC is seen and another band centered around 370 nm is observable with a continuous increase as the PVAc content increases. Although the PVAc exhibits the highest k values, all films display k below 1.6×10^{-4} in the visible and IR regions. Using the R spectra, the refractive index was determined using the following equation [19]: $n = \frac{1 + \sqrt{R}}{1 - \sqrt{R}}$. As seen from Fig. 4c, the films have $1.45 \leq n \leq 2.2$ in the visible and IR regions, and the n values increase with increasing PVAc content. The n of PVC at 500 nm is 1.54, which is very similar to that reported by ElSad et al. [18] (1.55). The n values of the films at 650 nm wavelength are listed in Table 1. These results indicate the suitability of PVAc-based blends

Fig. 3 a HR-TEM image for MgO NP, and FE-SEM images for b PVAc/PVC blend, c 10.0 wt% MgO/blend nanocomposite film. SEM images with higher magnification are found in the supplementary material file (Fig. S1)



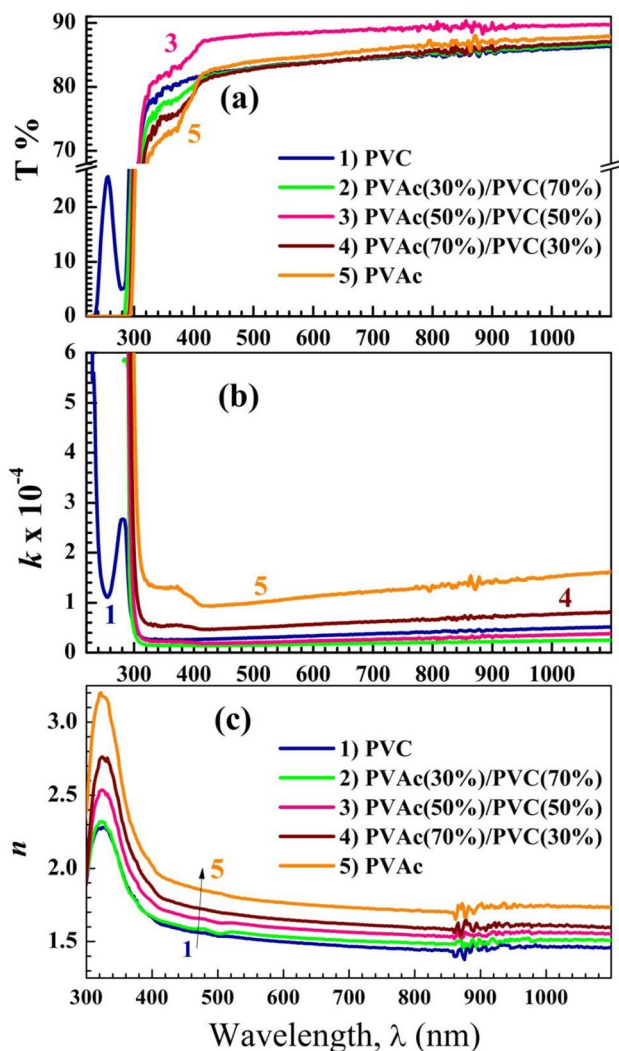


Fig. 4 Transmittance (a), the extinction coefficient (b), and the refractive index (c) of PVC, PVAc, and PVAc/PVC blends

in antireflective coating applications and high-refractive-index lenses.

Figure 5a, b displays the $T\%$ and k values of the PVAc (50%)/PVC (50%) blend loaded with 3.0, 5.0, and 10 wt% MgO NP. Incorporation of the nano-fillers at these content

Table 1 Transmittance and refractive index at 650 nm wavelength, direct (E_{gap}^{di}) and indirect (E_{gap}^{id}) bandgap for PVC, PVAc, and their blends

Bandgap		n at 650 nm	$T\%$ at 650 nm	Film
E_{gap}^{id}	E_{gap}^{di}			
4.81	5.10	1.48	84.23	PVC
4.20	4.25	1.52	84.20	PVAc(30%)/PVC(70%)
4.10	4.22	1.58	88.85	PVAc(50%)/PVC(50%)
3.90	4.13	1.63	84.17	PVAc(70%)/PVC(30%)
3.80	4.05	1.75	85.34	PVAc

ratios decreases the $T\%$ at $\lambda \geq 400$ nm from $\sim 90\%$ to be in the range of 27–62%, 16–45%, and 7–25%, respectively. The $T\%$ value at $\lambda = 650$ nm is listed in Table 2. MgO has UV blocking ability, where the $T\%$ of the blend decreased from $\sim 80\%$ in the UV region to values of 22, 12, and 5% upon doping with 3.0, 5.0, and 10 wt% MgO NP, respectively. In addition, loading MgO inside the blend matrix significantly increased k values to be in the range of $(0.25\text{--}1.25) \times 10^{-4}$. The free electrons of MgO can absorb the incident radiation. In addition, MgO NP can act as scattering centers and may increase the dispersion of light and cause the observed decrease in $T\%$ [20]. This is confirmed by plotting the recorded $R\%$ spectra of the nanocomposite films, see Fig. S2, where the $R\%$ values are greatly enhanced after doping with MgO. Additionally, a peak centered around 319 nm (3.78 eV) with a significantly improved intensity due to the UV blocking ability of MgO NP was also observed. These results indicate the possibility of improving PVAc and PVC industrial utilization for coatings, adhesives, and medical applications by loading MgO NP. Moreover, the n values of the nanocomposite films are significantly increased with the MgO ratio, see Fig. 6. For example, at $\lambda = 650$ nm, n increased from 1.58 to 2.48 at 10 wt% MgO NP content.

Utilizing Tauc's relation: $(ahv)^r = B(hv - E_g)$, where B is a constant and $r = 2$ and $\frac{1}{2}$ for the direct and indirect optical transitions, respectively, the direct (E_{gap}^{di}) and indirect (E_{gap}^{id}) energy bandgaps of PVC, PVAc, PVAc/PVC blends, and blends loaded with 3.0–10 wt% MgO are obtained by plotting $(ahv)^2$ and $(ahv)^{0.5}$ as a function of the photon energy (hv) as shown in Figs. 7a, b and 8a, b, respectively. Values of E_{gap}^{di} and E_{gap}^{id} have been obtained by extrapolating the linear portion of the curves to intercept the (hv) -axis at $(ahv)^2$ and $(ahv)^{0.5} = 0$ and their values are shown in Tables 1 and 2. The E_{gap}^{di} and E_{gap}^{id} of PVC are 5.10 and ~ 4.81 eV, respectively. Similarly, ElSad et al. [18] found these values as 5.14 and 4.5 eV. However, the E_{gap}^{di} and E_{gap}^{id} of PVAc are 4.05 and 3.8 eV, respectively, which are smaller than that reported by Abdelghany et al. [4], 5.09 and 4.78 eV. In addition, our results indicate that the E_{gap}^{di} and E_{gap}^{id} of the PVAc (50%)/PVC (50%), the blend is smaller (4.22 and 4.1 eV, respectively) than that reported for the same blend (5.09 and 4.68 eV). It is well-known that the materials' properties depend on the preparation method and the experimental conditions. The obtained results confirm that it is possible to control the bandgap structures of PVAc/PVC by adjusting the PVC and PVAc ratio in the blend. Moreover, MgO can make 3D networked structure inside the blend matrix and conduct paths that improve the semiconducting behavior of the blend, which reduced the E_{gap}^{di} and E_{gap}^{id} from 4.22 and 4.1 eV to 3.97 and 3.6 eV, respectively, as shown in Table 2.

From the quantum mechanical point of view, the optical dielectric loss ($\epsilon_{loss}^{op} = 2nk$) reflects the response of the

Fig. 5 UV–Vis-NIR transmittance spectra (a) and absorption index (b) of PVAc(50)/PVC(50%) blend and MgO/blend nanocomposites

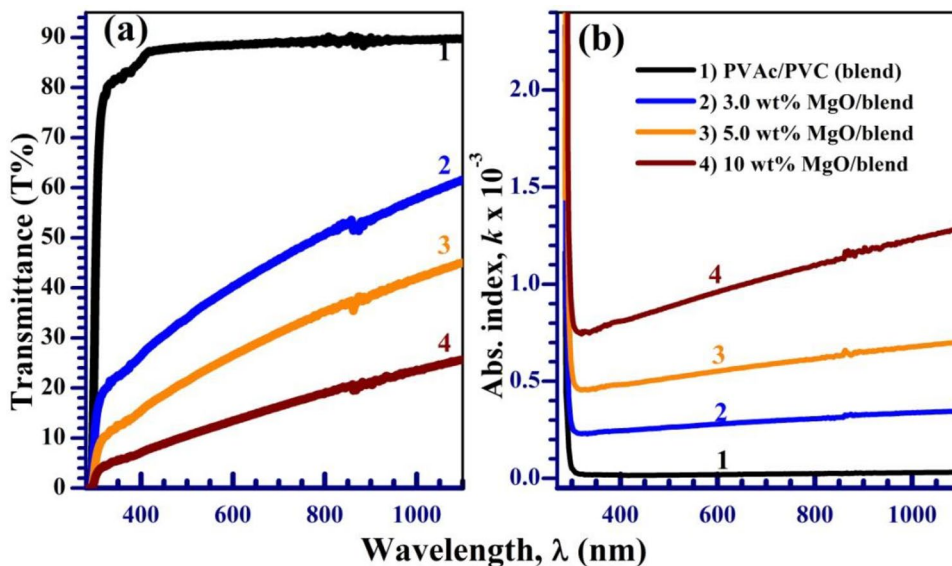


Table 2 Transmittance at 650 nm, refractive index (n) at 650 nm, indirect (E_{gap}^{id}) and direct (E_{gap}^{di}) bandgap, charge carrier/electron effective mass (N/m^*), and optical constants (E_o, E_d, λ_o and n_∞) of MgO/PVC/PVAc nanocomposites

n_∞	λ_o (nm)	E_d (eV)	E_o (eV)	$(N/m^*) \times 10^{-13}$	Bandgap (E_g) (eV)			n	T %	Film
					Dielectric loss	E_{gap}^{di}	E_{gap}^{id}			
2.312	299.6	17.46	4.016	6.08	4.28	4.22	4.10	1.58	84.25	PVAc/PVC (blend)
3.316	388.8	30.91	3.091	14.44	4.21	4.18	3.90	1.96	43.06	3.0 wt% MgO/blend
4.203	422.3	46.25	2.775	29.66	4.08	4.10	3.80	2.26	28.80	5.0 wt% MgO/blend
5.099	449.8	61.18	2.753	39.63	4.00	3.97	3.60	2.48	14.87	10 wt% MgO/blend

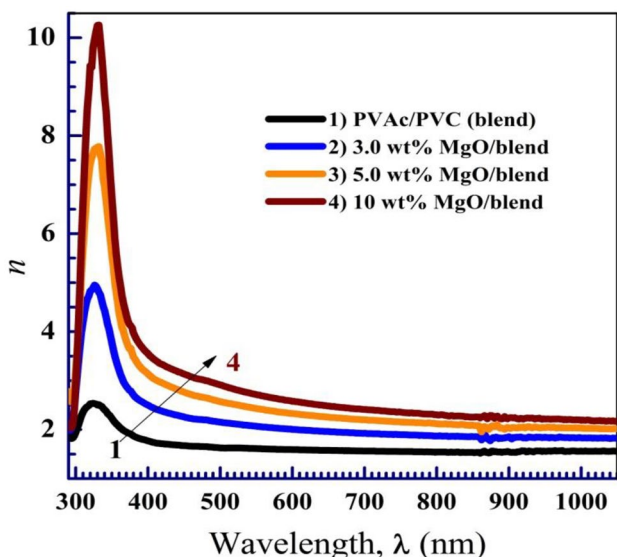
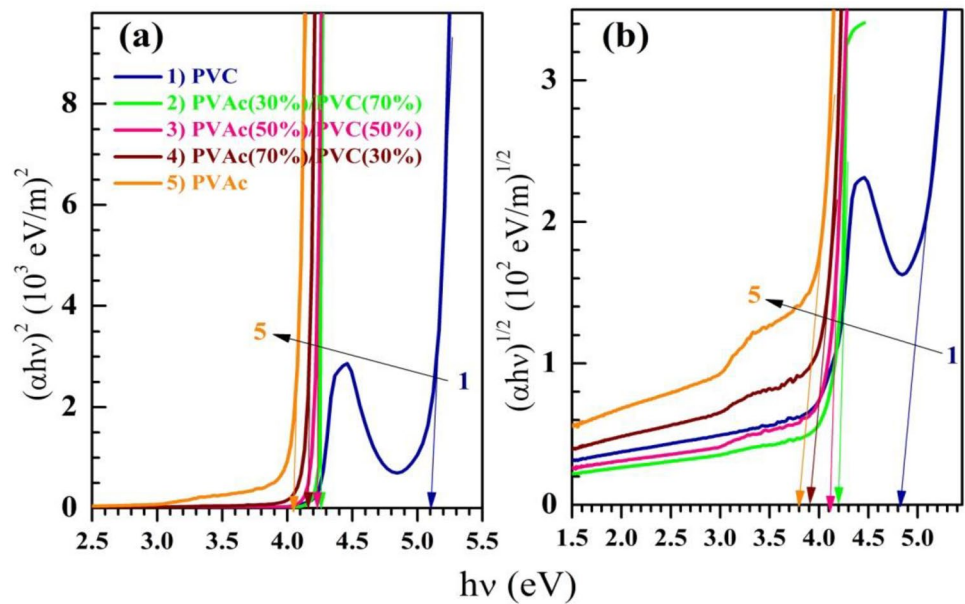


Fig. 6 The dependence of the refractive index on the incident wavelength for MgO/blend nanocomposites

incident electromagnetic photons to the electronic transitions and can be considered as an alternative to Tauc’s theory to obtain the bandgap of the material [20, 21]. Figure 8c displays the ϵ_{loss}^{op} vs. $h\nu$ plots for MgO/PVAc/PVC films. The PVAc/PVC blend has a bandgap of 4.28 eV, which was reduced to 4.0 eV after doping with 10 wt% MgO NP, as listed in Table 2. These values are close to the estimated E_{gap}^{di} values, the difference does not exceed 1.4%. Therefore, ϵ_{loss}^{op} and Tauc’s equations are equivalent for the effective calculation of the bandgap. As seen in Fig. 8c, the ϵ_{loss}^{op} spectra of MgOPVAc/PVC films exhibit a peak at ~ 3.78 eV, which is improved with increasing MgO content from 3.0 to 10 wt%. This peak is related to the UV blocking ability of MgO NP seen in Fig. S2.

The N/m^* ratio (the carriers’ concentration/the electron effective mass), the dispersion energy (E_d), the average excitation energy for electronic transitions (E_o), the long-wavelength refractive index (n_∞), and the average inter-band oscillator wavelength (λ_o) are important parameters

Fig. 7 Direct (a) and indirect (b) optical bandgap of PVC, PVAc, and PVAc/PVC blends with different constituents



in designing optical and optoelectronic devices. The decrease of n with λ , see Fig. 6b, is fitted by the Wemple & Di-Domenico model, and these parameters can be determined by considering the following dispersion relations [22, 23]:

$$n^2 = \varepsilon_l - \lambda^2 \left(\frac{e^2}{\pi c^2} \right) \left(\frac{N}{m^*} \right) \quad (1)$$

$$\frac{(n_\infty^2 - 1)}{(n^2 - 1)} = 1 - \left(\frac{\lambda_o}{\lambda} \right)^2 \quad (2)$$

$$n^2 = 1 + \frac{E_d E_o}{E_o^2 - (hv)^2} \quad (3)$$

where ε_L is the lattice dielectric constant, e is the electron charge, and c is the velocity of light. Figure 9 a shows the plots of n^2 vs. λ^2 for the PVAc (50%)/PVC (50%) blend and the 3–10 wt% MgO- doped blend. The slopes of the linear lines give the (N/m^*) . As listed in Table 2, the N/m^* significantly increased from 6.08×10^{-13} to 39.63×10^{-13} , which supports the suggestion that MgO increases the amorphous nature (as seen from XRD results), defects, and form pathway via a 3D connected network to facilitate the charge mobility. The n_∞ and λ_o parameters were determined from the slopes and the intercepts of $(n^2-1)^{-1}$ vs. λ^{-2} plots shown in Fig. 9b, and their values are given in Table 2. In addition, the E_d and E_o values were obtained from the intercepts and slopes of the linear portions of the $(n^2-1)^{-1}$ vs. $(hv)^2$ plots, as shown in Fig. 9c. The induced modifications of these parameters confirm the effectiveness of MgO NP in the optical properties and optical constants of the PVAc/PVC blend.

3.3 Stress–Strain Behavior of Nanocomposite Films

Introducing nano-sized fillers usually increases the matrix/reinforcement interfaces in the polymer nanocomposites (PNC), which influences the overall performance of the material. The strength of PVAc/PVC blends, as well as the MgO/blend, depends on the properties of the blend components, the adhesion between the blend and the fillers, and the distribution of the filler. Figure 10a, b shows the stress–strain behaviors of PVC, PVAc, PVAc (50%)/PVC (50%) blend, and the blend loaded with 3.0, 5.0, and 10 wt% MgO NP. The obtained mechanical properties are listed in Table 3. The blend exhibits the highest ultimate tensile stress, $U\sigma_M = 23.12$ MPa, compared with that of PVC and PVAc. The other mechanical properties, tensile modulus (E_t), stress at break (σ_B), strain at break (ε_B), strain at tensile strength (ε_M), and toughness are between those of PVC and PVAc. The obtained results confirm that mixing PVAc with PVC yields a blend with suitable properties for different applications. In a previous report [24], the ε_B of PVC was 43% and decreased 11–15% after mixing with 20–40% CuO or PbO nano-fillers. Blending polyurethane (at 0–75%) with PVC increased the toughness and elongation at the break, whereas the tensile strength was decreased [25].

The incorporation of 10 wt% MgO NP inside the blend matrix improved the tensile strength (σ_M) from 62.6 N to 95.9 N, the $U\sigma_M$ from 23.12 to 25.44 MPa, and the σ_B from 8.9 to 18.4 MPa. Increasing the tensile strength with the increase in MgO content demonstrates that the MgO acts like a pillar in the polymer matrix. The toughness of the blend is 20.01 MPa, increased to 23.99 MPa at 3.0 wt% MgO NP content, but decreased to 17.83 and 16.87 MPa upon increasing the MgO content to 5.0 and 10 wt%, respectively.

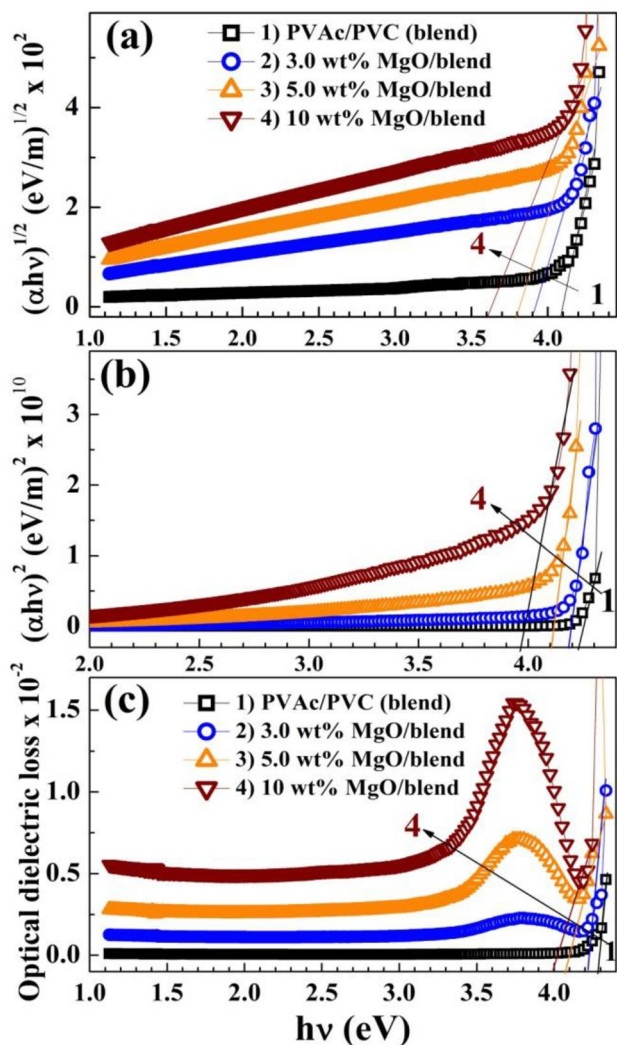


Fig. 8 Indirect (a) and direct (b) optical bandgap determination using Tauc's plots, and from the optical dielectric loss (c) for PVAc/PVC blend with 3.0–10 wt% MgO

In addition, MgO fillers make the region between the yield point and the $U \sigma_M$ more linear. The efficient transformation of the applied stress from the PVAc/PVC blend to the stronger MgO NP and the improvement in the strength of nanocomposite films are owing to the good compatibility between MgO and the blend chains, the higher interfacial area offered by nano-sized fillers, and the induced reinforcement in the nanocomposites [3, 16]. The elongation at break, ϵ_B , exhibits a continuous decrease with increasing MgO NP content, which may be attributed to the decrease in the molecular mobility due to the physical reaction between the fillers and the blend molecular chain that stiffens the blend matrix. Furthermore, increasing MgO content enhances the tensile modulus (E_t) of the blend from 148 to 1730 MPa which reflects the increasing rigidity of the blend. These

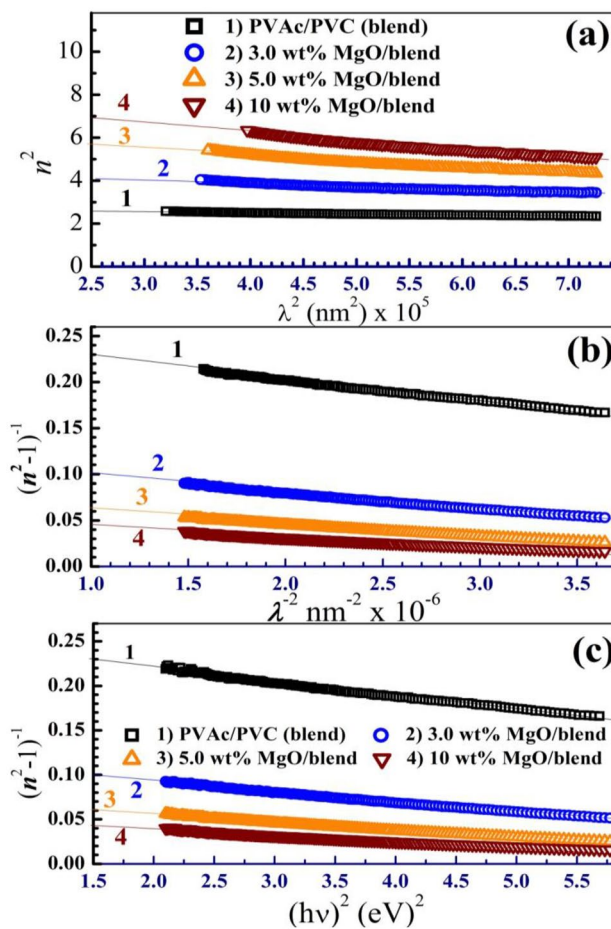


Fig. 9 n^2 vs. λ^{-2} (a), $\frac{1}{(n^2-1)}$ vs $\frac{1}{\lambda^2}$ (b) and $\frac{1}{(n^2-1)}$ vs $(hv)^2$ (c) for optical constants determination, according to Eqs. (1), (2) and (3), for MgO/blend films

improved parameters make the MgO/blend nanocomposite films candidate for carrying purposes and food packaging applications.

3.4 Antibacterial Studies

The antibacterial activity percentage (%) was calculated from the following relation [4]:

$$\% \text{ Activity Index} = \frac{\text{zone of inhibition by test sample (diameter)}}{\text{zone of inhibition by standard (diameter)}} \times 100 \tag{4}$$

Table 4 and Fig. 11 reveal the diameter of the inhibition zone and the activity index of the studied blend doped with different concentrations of synthesized MgO NP. All graphs were plotted on the same activity index scale to show the behavior of the doped sample against different grams. In addition, the photos of the inhibition halos related to

Fig. 10 Stress–strain curves of (a) PVC, PVAc, and PVAc (50%)/PVC (50%) blend and (b) the blend loaded with 3.0–10 wt% MgO

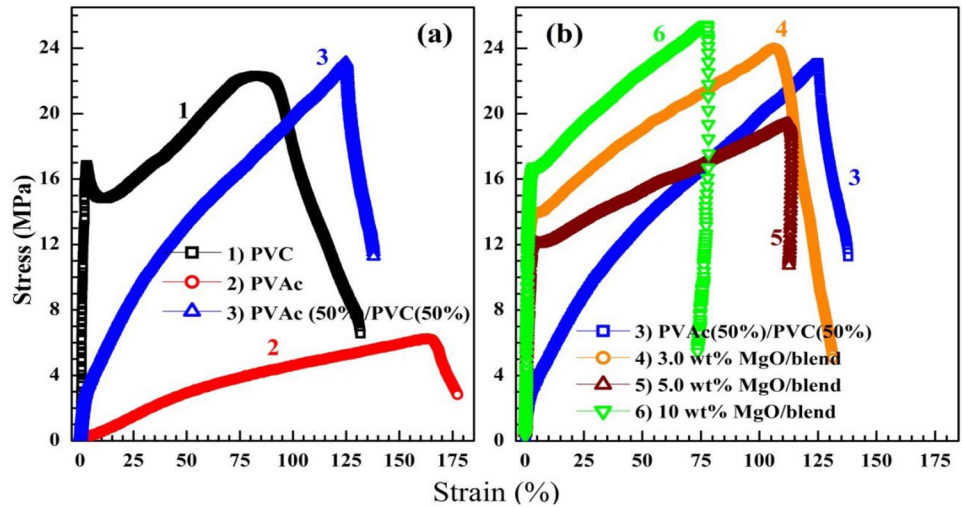


Table 3 Mechanical properties of PVAc, PVC, blend (50%/50%), and the blend loaded with 3.0–10 wt% MgO: tensile modulus (E_t), tensile strength (σ_M), ultimate tensile stress ($U \sigma_M$), strain at tensile strength (ϵ_M), stress at break (σ_B), strain at break (ϵ_B), and toughness

Toughness MPa	ϵ_B (%)	σ_B (MPa)	ϵ_M (%)	$U \sigma_M$ (MPa)	σ_M (N)	σ_y (MPa)	E_t (MPa)	Sample
22.40	99.4	10.7	49.2	22.33	71.2	17.5	1400	PVC
6.77	172.0	8.62	167.1	6.24	29.3	0.433	7.27	PVAc
20.01	132.3	8.9	121.2	23.12	62.6	-	148	Blend (50%/50%)
23.99	129.7	16.7	119.4	24.01	90.9	-	760	3.0 wt% MgO/blend
17.83	108.4	17.2	108.3	19.41	76.2	13.5	311	5.0 wt% MgO/blend
16.87	98.0	18.4	99.0	25.44	95.9	16.4	1730	10.0 wt% MgO/blend

Table 4 Diameter (D) of inhibition zone and activity index (A) of studied samples against different pathogenic grams

Compound	<i>E. coli</i>		<i>S. aureus</i>		<i>C. albicans</i>	
	D (mm)	A (%)	D (mm)	A (%)	D (mm)	A (%)
PVAc/PVC (blend)	9.0	25	8.0	30	8	33
3.0 wt% MgO/blend	10.5	33	8.5	30	8	33
5.0 wt% MgO/blend	11.0	36	9.0	33	8	33
10.0 wt% MgO/blend	12.0	39	9.0	33	9	37
Cefotax	36.0	100	30.0	100	27	100

the antibacterial activity of of PVAc(50)/PVC(50%) blend and MgO/blend nanocomposites are shown in Fig. S3. The pure blend exhibits $A = 25\%$, 30% , and 33% for *E. Coli*, *S. Aureus*, and *C. Albicans*, respectively. For the PNCs films, $A\%$ towards *E. Coli* increased significantly with increasing MgO NP loading in the range of 3.0–10.0 wt% to about 40% percent of that of the standard drug (Cefotax) used. While a nearly constant behavior against both *S. Aureus* and *C.*

Albicans with a step increase in the sample contains high content of MgO NP to about 33% and 37%, respectively. Such behavior may be attributed to the agglomeration of NP in the higher filling level or to the unreacted portion of filler causing an increase in the reactive oxygen species. These results illustrate the possibility of extending the use of MgO/PVAc/PVC films of improved mechanical properties for carrying purposes and food packaging applications.

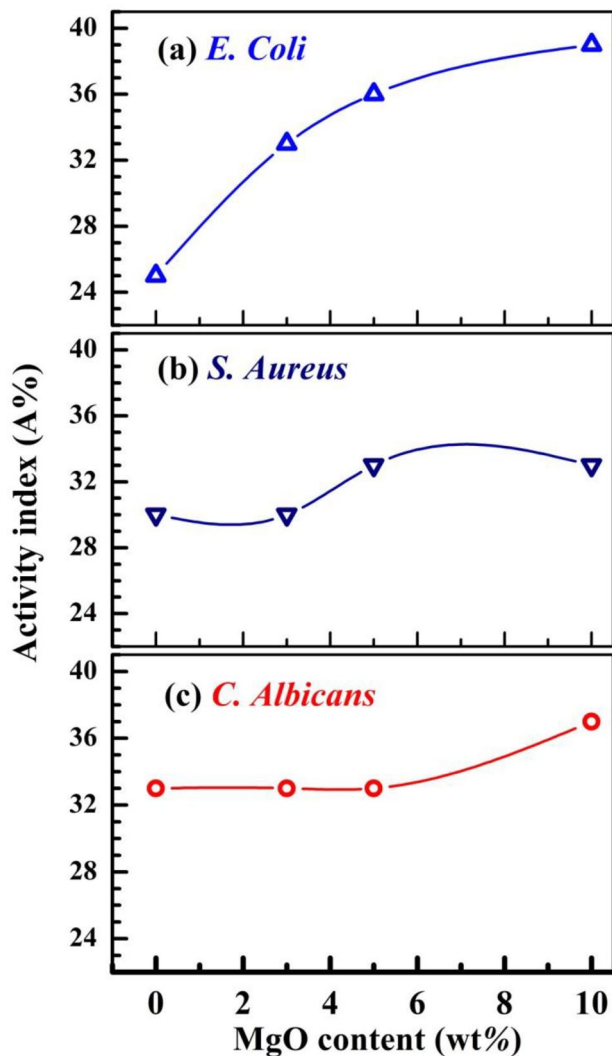


Fig. 11 a–c The gradual change in the activity index of studied samples

4 Conclusions

MgO NP, PVAc/PVC, and MgO/PVAc/PVC nanocomposites were prepared by sol–gel and solution casting/evaporation methods. FTIR confirmed the good miscibility between PVAc and PVC, where the band at 1720 cm^{-1} (of $\text{C}=\text{O}$ of PVAc) and the peak at 1254 (of the acetate structure) cm^{-1} were strengthened with increasing PVAc content in the blend. In addition, the result confirmed the hydrogen bonding formation between the MgO and CH_3COO groups of the PVAc in the blend. XRD showed that PVAc/PVC blend maintained its amorphous structure without affecting the crystal structure of the sol–gel prepared MgO NP which was of periclase phase and had an

average crystallite size D of ~ 18.8 nm. SEM images showed that the blend film has a smooth and crack-free surface, confirming the good miscibility and homogeneity of the blend. The UV–vis–NIR study showed that the blend of composition PVAc (50%)/PVC (50%) has the highest transmittance and a moderate refractive index of $n = 1.58$. The $E_{\text{gap}}^{\text{di}}$ and $E_{\text{gap}}^{\text{id}}$ of the PVC were 5.10 and 4.81 eV, respectively, decreased with increasing PVAc content to 4.05 and 3.8 eV, respectively, at 100% PVAc. Doping with 3.0–10 wt% MgO NP improved the ability of the blend to block UV radiation and decreased the $T\%$ from 84.25 to 14.87% at $\lambda = 650$ nm. In addition, the doping decreased the $E_{\text{gap}}^{\text{di}}$ and $E_{\text{gap}}^{\text{id}}$ of the blend to 3.97 and 3.60 eV, respectively. There was a consistency between $\epsilon_{\text{loss}}^{\text{op}}$ and Tauc's method in deriving the $E_{\text{gap}}^{\text{di}}$ values. The N/m^* was greatly increased from 6.08×10^{-13} to 39.63×10^{-13} upon doping with 10 wt% MgO. Moreover, the other optical constants; E_o , E_d , λ_o , and n_∞ were significantly improved with doping. The stress–strain measurements showed that PVAc (50%)/PVC (50%) exhibited improved mechanical properties compared with the individual polymers, PVC and PVAc. Moreover, doping with MgO nano-fillers improved σ_M from 62.6 to 95.9 N, the $U\sigma_M$ from 23.12 to 25.44 MPa, and the σ_B from 8.9 to 18.4 MPa, which demonstrates that the MgO acts like a pillar in the polymer matrix. This is owing to the efficient transformation of the applied stress from the blend to MgO NP, the good compatibility between MgO and the blend chains, the higher interfacial area offered by nano-sized fillers, and the induced reinforcement in the nanocomposites. The toughness of the blend is 20.01 MPa, increased to 23.99 MPa at 3.0 wt% MgO NP content. The elongation at break exhibits a continuous decrease with increasing MgO NP content, which may be attributed to the decrease in the molecular mobility due to the physical reaction between the fillers and the blend molecular chain that stiffens the blend matrix. The diameter of the inhibition zone and activity index of the PNCs towards *E. Coli*, *S. Aureus*, and *C. Albicans* were enhanced. The improvements in the optical, mechanical properties, and antibacterial activity suggest the suitability of the nanocomposites in some optical components and food packaging applications and the carrying purposes.

Supplementary Information The online version contains supplementary material available at <https://doi.org/10.1007/s13538-022-01156-x>.

Funding Open access funding provided by The Science, Technology & Innovation Funding Authority (STDF) in cooperation with The Egyptian Knowledge Bank (EKB).

Data Availability No new data generated or analyzed.

Declarations

Conflict of Interest The authors declare no competing interests.

Open Access This article is licensed under a Creative Commons Attribution 4.0 International License, which permits use, sharing, adaptation, distribution and reproduction in any medium or format, as long as you give appropriate credit to the original author(s) and the source, provide a link to the Creative Commons licence, and indicate if changes were made. The images or other third party material in this article are included in the article's Creative Commons licence, unless indicated otherwise in a credit line to the material. If material is not included in the article's Creative Commons licence and your intended use is not permitted by statutory regulation or exceeds the permitted use, you will need to obtain permission directly from the copyright holder. To view a copy of this licence, visit <http://creativecommons.org/licenses/by/4.0/>.

References

1. Y. Li, C. Han, L. Xiao, Y. Yu, G. Zhou, M. Xu, Miscibility, morphology, and properties of poly(butylene succinate)/poly(vinyl acetate) blends. *Colloid Polym. Sci.* **299**, 105–116 (2021). <https://doi.org/10.1007/s00396-020-04773-7>
2. R.K. Goyal, *Nanomaterials and nanocomposites: synthesis, properties, characterization techniques, and applications* (1st ed.). CRC Press. (2017) <https://doi.org/10.1201/9781315153285>
3. C. Swaroop, M. Shukla, Nano-magnesium oxide reinforced polylactic acid biofilms for food packaging applications. *Int. J. Biolog. Macromol.* **113**, 729–736 (2018). <https://doi.org/10.1016/j.ijbiomac.2018.02.156>
4. A.M. Abdelghany, M.S. Meikhaail, N. Asker, Synthesis and structural-biological correlation of PVC/PVAc polymer blends. *J. Mater. Res. Technol.* **8**(5), 3908–3916 (2019). <https://doi.org/10.1016/j.jmrt.2019.06.053>
5. I. Hammami, K. Benhamou, H. Hammami, S. SoretoTeixeira, M. Arous, H. Kaddami, M.P.F. Graça, L.C. Costa, Electrical, morphology and structural properties of biodegradable nanocomposite polyvinyl-acetate/cellulose nanocrystals. *Mater. Chem. Phys.* **240**, 122182 (2020). <https://doi.org/10.1016/j.matchemphys.2019.122182>
6. K.Č Barabasova, S. Holešova, M. Bily, M. Hundakova, CuO and CuO/vermiculite based nanoparticles in antibacterial PVAc nanocomposites. *J. Inorg. Organomet. Polym. Mater.* **30**, 4218–4227 (2020). <https://doi.org/10.1007/s10904-020-01573-y>
7. H.U. Khan, M.T. Jan, M. Iqbal, M. Shah, I. Ullah, J. Khan, K. Mahmood, A. Niaz, M. Tariq, Synthesis, characterization and electrical conductivity of silver doped polyvinyl acetate/graphene nanocomposites: a novel humidity sensor. *Z. Phys. Chem.* **234**(1), 27–43 (2020). <https://doi.org/10.1515/zpch-2018-1302>
8. M. Dogan, M. Turan, P.T. Beyli, Z. Bicil, B.K. Kızılduman, Thermal and kinetic properties of poly(vinylacetate)/modified MWCNT nanocomposites. *Fuller. Nanotub. Carbon Nanostruct.* **29**(6), 475–485 (2021). <https://doi.org/10.1080/1536383X.2020.1860945>
9. S. Saritas, S. Essiz, B. Sari, Synthesis and characterization of foldable and magnetic field-sensitive, freestanding poly(vinyl acetate)/poly(vinyl chloride)/polyfuran composite and nanocomposite films. *J. Magnet. Mater.* **433**, 120–130 (2017). <https://doi.org/10.1016/j.jmmm.2017.03.007>
10. Y. Wang, C. Cen, J. Chen, L. Fu, MgO/carboxymethyl chitosan nanocomposite improves thermal stability, waterproof and antibacterial performance for food packaging. *Carbohydr. Polym.* **236**, 116078 (2020). <https://doi.org/10.1016/j.carbpol.2020.116078>
11. N.-Y T. Nguyen, N. Grelling, C.L. Wetteland, R. Rosario, H. Liu, Antimicrobial activities and mechanisms of magnesium oxide nanoparticles (nMgO) against pathogenic bacteria, yeasts, and biofilms. *Sci. Rep.* **8**, 16260 (2018). <https://doi.org/10.1038/s41598-018-34567-5>
12. S.N. Hosseini, S. Pirsra, J. Farzi, Biodegradable nano composite film based on modified starch-albumin/ MgO; antibacterial, antioxidant and structural properties. *Polym. Testing* **97**, 107182 (2021). <https://doi.org/10.1016/j.polymertesting.2021.107182>
13. S. Rajendran, R. Kannan, O. Mahendran, Ionic conductivity studies in poly (methylmethacrylate)-polyethylene oxide hybrid polymer electrolytes with lithium salts. *J. Power Sources* **96**, 406–410 (2001). [https://doi.org/10.1016/S0378-7753\(00\)00573-5](https://doi.org/10.1016/S0378-7753(00)00573-5)
14. S. Ramesh, K.H. Leen, K. Kumuth, A.K. Arof, FTIR studies of PVC/PMMA blend based polymer electrolytes. *Spectrochim. Acta, Part A* **66**, 1237–1242 (2007). <https://doi.org/10.1016/j.saa.2006.06.012>
15. I.S. Elashwai, N.A. Hakeem, E.M. Abdelrazek, Spectroscopic and thermal studies of PS/PVAc blends. *Physica B* **403**, 3547–3552 (2008). <https://doi.org/10.1016/j.physb.2008.05.024>
16. A. Abdolmaleki, S. Mallakpour, H. Tabebordbar, Study on morphology, thermal, mechanical and Cd(II) adsorption properties of PVC/ α -MnO₂-stearic acid nanocomposites: production and application. *J. Polym. Res.* **23**, 260 (2016). <https://doi.org/10.1007/s10965-016-1154-7>
17. A.M. El Sayed, W.M. Morsi, Dielectric relaxation and optical properties of polyvinyl chloride/lead monoxide nanocomposites. *Polym. Compos.* **34**, 2031 (2013). <https://doi.org/10.1002/pc.22611>
18. R.A. Elsad, K.A. Mahmoud, Y.S. Rammah, A.S. Abouhaswa, Fabrication, structural, optical, and dielectric properties of PVC-PbO nanocomposites, as well as their gamma-ray shielding capability. *Rad. Phys. Chem.* **189**, 109753 (2021). <https://doi.org/10.1016/j.radphyschem.2021.109753>
19. N.H. El Fewaty, A.M. El Sayed, R.S. Hafez, Synthesis, structural and optical properties of tin oxide nanoparticles and its CMC/PEG-PVA nanocomposite films. *Polym. Sci. Ser. A* **58**(6), 1004–1016 (2016). <https://doi.org/10.1134/S0965545X16060055>
20. A.M. El Sayed, S. Saber, Structural, optical analysis, and Poole-Frenkel emission in NiO/CMC-PVP: bio-nanocomposites for optoelectronic applications. *J. Phys. Chem. Solids* **163**, 110590 (2022). <https://doi.org/10.1016/j.jpcs.2022.110590>
21. G. Mohammed, A.M. El Sayed, Structural, morphological, optical and dielectric properties of M³⁺/PVA/PEG SPE Films (M = La, Y, Fe or Ir). *Polym. Adv. Technol.* **30**(3), 698–712 (2019). <https://doi.org/10.1002/pat.4508>
22. A.M El Sayed, Opto-structural and surface properties of silkworm-like nickel oxide thin films, *Mater. Res. Express* **6**, 116423 (2019). <https://doi.org/10.1088/2053-1591/ab4663>
23. H. Khmissi, A.M. El Sayed, M. Shaban, Structural, morphological, optical properties and wettability of spin-coated copper oxide; influences of film thickness, Ni, and (La, Ni) co-doping. *J. Mater. Sci.* **51**, 5924 (2016). <https://doi.org/10.1007/s10853-016-9894-7>
24. Y.M. Abbasi, A.M. EL-Khatib, M.S. Badawi, M.T. Alabsy, O.M. Hagag, Gamma attenuation through nano lead – nano copper PVC composites, *Nucl. Technol. Rad. Protect.* **36**(1), 50–59 (2021). <https://doi.org/10.2298/NTRP210110001A>
25. A.M. Hezma, I.S. Elashmawi, A. Rajeh, M. Kamal, Change spectroscopic, thermal and mechanical studies of PU/PVC blends. *Physica B* **495**, 4–10 (2016). <https://doi.org/10.1016/j.physb.2016.04.043>

Publisher's Note Springer Nature remains neutral with regard to jurisdictional claims in published maps and institutional affiliations.